



TURBULENCE MODEL ASSESSMENT OF THE SEPARATED FLOW IN THE STANFORD DIFFUSER

Mario Bonnici, Simon Prince & Kevin Garry

Applied Aerodynamics Group, Centre for Aeronautics, Cranfield University, UK

Abstract

The computational prediction of separated turbulent flows in internal ducts is a well-known challenging problem. The flow separation within the diffuser sections of wind tunnels is a significant problem and was the motivation for this study which aimed to identify the most accurate turbulence model for the prediction of the separated flow regions in a large industrial wind tunnel. To investigate this problem, the Stanford diffuser developed by Cherry et al., was used as a benchmark to compare simulations with different turbulence models. Corner flow separations, with the associated decrease in static pressure rise, total pressure losses and flow unsteadiness are common in rectangular diffusers. Results from the Stanford diffuser test-case show that linear eddy-viscosity models fail to predict flows in highly asymmetric diffusers due to their over-sensitivity to transverse pressure gradients. On the other hand, Reynolds stress model (RSM) simulations, particularly with the Gibson and Launder (GL-RSM) formulation are in better qualitative and quantitative agreement with the experimental data due to the anisotropic nature of their Reynolds stress formulation.

Keywords: Diffuser, Flow Separation, Secondary Flow, Turbulence Models.

1. Introduction

A diffuser is a device used in aerodynamics to convert dynamic pressure into static pressure. The importance of this process and its impact on efficiency have long been recognised in the field of turbomachinery. The performance of a diffuser is dependent on both geometric and flow variables. Important geometric variables are the wall divergence angles, the length-to-inlet height ratio and the inlet aspect ratio. Flow variables include the thickness of the inlet boundary layer, turbulence intensity and Reynolds number. Due to the large number of flow and geometric variables, it is difficult to determine a generalised theory for diffusers since large amounts of data are needed to systematically study the effect of a single variable [1].

The main challenge when designing diffusers is to maximise the pressure recovery while avoiding massive flow separation due to a strong adverse pressure gradient. Therefore, in many cases, diffusers are operated close to or at their stall limit. The development of the boundary layer over the walls of the diffuser is the cause of viscous losses. Corner separations are also a typical flow feature of rectangular diffusers where the intersecting boundary layer separates under the effect of an adverse pressure gradient. Apart from causing total pressure losses, regions of reversed flow also reduce the effective area of the diffuser, thus lowering static pressure recovery [2].

Flow separation within the diffuser section of a wind tunnel is a significant problem due to total pressure losses and flow unsteadiness associated with separations. Unsteadiness in the test-section flow can affect the accuracy of measurements and limit the ability to undertake studies such as aeroacoustics studies and boundary-layer control studies [3, 4]. This study aimed to identify the most accurate turbulence model for the prediction of separated flow regions in a large industrial wind tunnel. Detailed numerical analysis could then be used to aid in the development and sighting of flow control devices in the diffuser to alleviate the effects of flow separation. With no experimental data from the diffuser available for this wind tunnel, it was necessary to undertake a validation exercise using a suitable

experimental database for a representative diffuser flow. The Stanford diffuser, developed by Cherry et al. (2006), was used as a benchmark due to the detailed flow measurements acquired and the unambiguous boundary conditions set [8].

2. Literature Review

Fox et al. (1962), at Stanford University, were the first to identify different diffuser flow regimes by performing experiments on two-dimensional (2-D) diffusers with high aspect ratios [5]. The length-to-inlet height ratio, N/W_1 , and total divergence angle, θ , were varied, and the state of diffuser flow was observed. Transition lines were then established between different regimes (Figure 1). Line A-A marks the occurrence of transitory stall which is generally unstable. When line B-B is crossed, the flow regime changes to fully developed stall which is characterised by stable reversed flow over the whole length of one wall. Line C-C indicates the transition to jet flow where the flow separates from all of the walls and the core flow acts like a free jet [5].

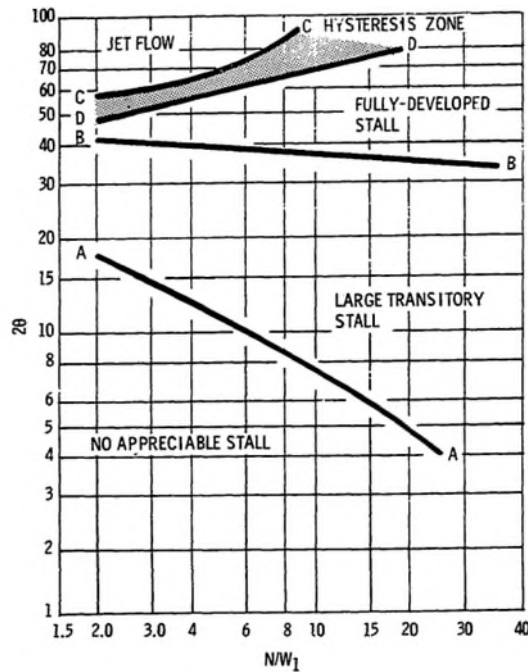


Figure 1: Flow regimes in 2-D diffusers [5].

Although flow is naturally three-dimensional, literature associated with 3-D diffuser flow is limited compared with planar diffusers. In 2-D flows separation occurs at regions of zero wall shear stress. However, in 3-D flows, separation can also occur at singular points (saddle points) and convergence lines emanating from these points [6]. Moreover, the geometry and viscous nature of fluids leads to corner effects and transverse pressure gradients which greatly complicate the analysis. In general, more detailed turbulence modelling is required in internal flows, compared to external flows where the role of turbulence is significant only in the boundary layer and at discontinuities on surfaces [7].

2.1 The Stanford Diffuser

A number of experiments have been carried out in order to study flow separation in 3-D diffusers. In the majority of these studies, the Stanford diffuser was used as a benchmark. The Stanford diffuser rig, the schematic diagram for which is presented in figure 2, is a three-dimensional (3-D) duct whose side wall and upper wall are deflected to form a diffuser and has been investigated experimentally by Cherry et al. (2006). The objective was to study the physics of flow separation due to an adverse pressure

gradient at the intersection of two deflected walls [8].

The tests were conducted in recirculating water with a Reynolds number of 10000 using magnetic resonance velocimetry (MRV). The bulk velocity in the inflow duct was 1 m/s. Fully developed conditions were obtained at the inlet of the diffuser using a long inflow duct. The uncertainty in axial velocity measurements was calculated to be less than 2% with a 95% confidence interval [8, 9].

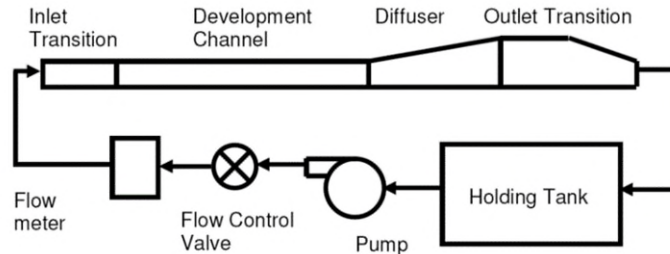


Figure 2: Schematic diagram of the experimental flow system [10].

The diverging walls of a diffuser impose an adverse pressure gradient and the flow decelerates. The Stanford diffuser was characterised by 3-D boundary layer separation. The separation bubble started in the upper-right corner and spread along the upper wall (Figure 3). Figure 4 shows the velocity component in a normal-to-wall plane of the inflow duct of the Stanford diffuser. The turbulent boundary layers interacted together to form a secondary flow in the plane normal to the flow. This secondary current transported momentum to the corners of the duct forming vortices on each side of the jet. Despite the low intensity of these secondary currents (maximum in-plane velocity magnitude of 2% of the axial bulk velocity), the effect on separation development was significant [8, 9, 10].

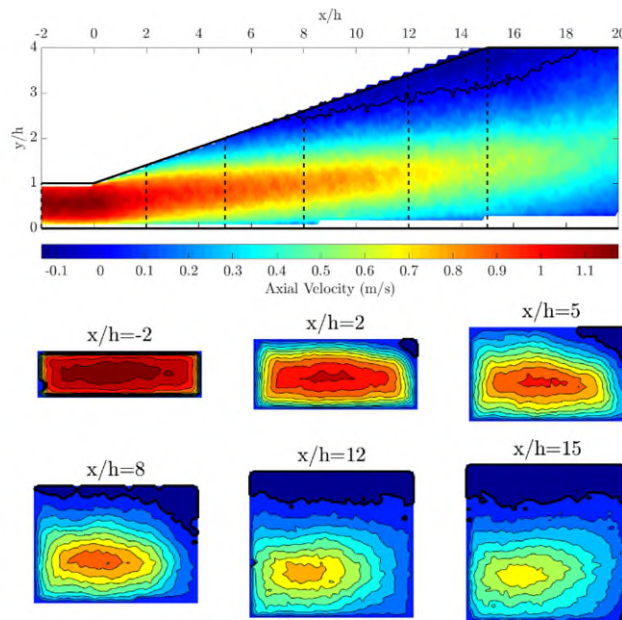


Figure 3: Velocity measurements in the Stanford diffuser. Top: Axial velocity contours on the central plane of the diffuser. Bottom: Axial velocity contours on cross-sectional slices along the diffuser. The black line marks the zero streamwise velocity contour [8].

2.2 Secondary Flow

Secondary flow in square ducts was first observed by Nikuradse (1926) who discovered that contours of constant velocity were distorted towards the corners. The existence of secondary currents was confirmed by subsequent flow visualisation of two helical vortices near the corner region divided by a corner bisector [11]. Prandtl (1953) postulated that the isotach distortion was due to fluid flow from regions of high shear stress to the interior and from the interior to regions of low shear stress (e.g. the corners of the duct) [12]. Prandtl also postulated that these currents were due to turbulent fluctuations tangential to the isotachs giving a net flow normal to the isotach directed from the concave towards the convex side. The assumption that the flow circuits are associated with curvature reversal of the isotach would require a double circulation in a rectangular duct as shown in Figure 5. Hoagland (1960) only measured one flow circuit near the corner in the trapezoidal sector when measuring secondary currents using a hot-wire yaw meter [13]. However, the magnitude of this circulation is very small and it is possible that it was not detected by the measuring instrument.

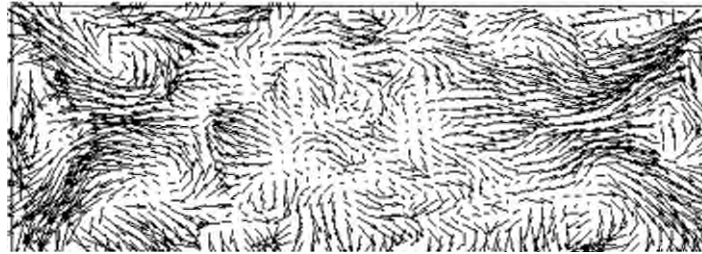


Figure 4: Experimental secondary flow currents in the inflow duct of the diffuser [8].

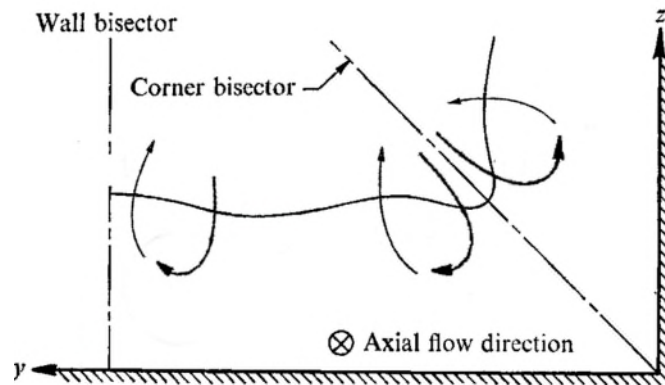


Figure 5: Contour of constant velocity pattern for flow near a corner [12].

Brundrett and Baines (1963) showed that gradients in Reynolds stresses in the plane normal to the bulk velocity give rise to a source of streamwise vorticity [14]. Consider flow in a non-circular duct where x defines the coordinate in the direction of the bulk flow and y and z are orthogonal coordinates. The velocity component U describes the primary flow and components V and W describe the secondary flow. The mean flow vorticity equation about the x -axis is given by [19],

$$\rho V \frac{\partial \Omega_x}{\partial x} - \rho W \frac{\partial \Omega_x}{\partial x} = \frac{\partial^2}{\partial y \partial z} (\tau_{zz} - \tau_{yy}) - \left(\frac{\partial^2}{\partial y^2} - \frac{\partial^2}{\partial z^2} \right) \tau_{yz} + \mu \left(\frac{\partial^2 \Omega_x}{\partial y^2} + \frac{\partial^2 \Omega_x}{\partial z^2} \right). \quad (1)$$

The terms on the left-hand side of Equation 1 represent convection of vorticity due to secondary flow. The last term on the right-hand side of the equation describes the diffusion of vorticity from regions of high intensity to regions of low intensity due to viscosity. The effect of this process is to make vorticity uniform over the duct's cross-section. In a laminar flow, these are the only terms in the equation; therefore, secondary flow cannot occur in a steady flow since these mechanisms can only transport and diffuse vorticity [14].

On the other hand, in turbulent flows, the presence of Reynolds stresses gives rise to a production term in the vorticity equation; thus, secondary flow is possible in a uniform flow. The secondary flow transports vorticity from regions of production to regions of diffusion. A necessary condition for secondary flow is that the axial velocity, U , should give rise to a non-zero Reynolds stress difference $\tau_{zz} - \tau_{yy}$; otherwise τ_{yz} is zero and the production terms vanish. In non-circular ducts, $\tau_{zz} - \tau_{yy} = 0$, hence secondary flow is generated [14, 15].

3. Separated Flow in the Stanford Diffuser – Comparing Turbulence Models

Simulations of separated flow in the Stanford diffuser were carried out. Validation was implemented by comparing results obtained using the commercial code FLUENT® with results presented in ERCOFTAC (European Research Community on Flow, Turbulence and Combustion) Workshops on Refined Turbulence Modelling. The effects of using various RANS turbulence models on the velocity and pressure development within the diffuser were studied. This case study was chosen since it provides a rigorous test for 3-D flow separation and the inlet boundary conditions are unambiguous since the flow was fully developed. The flow in the Stanford diffuser belongs to a class of mildly separated flows. The flow is stable, and separation occurs due to an adverse pressure gradient. In contrast with globally unstable flows, such as geometry-induced separated flows, a more exacting near-wall treatment is generally required. Figure 6 presents the geometry of the diffuser used in the Stanford experiments.

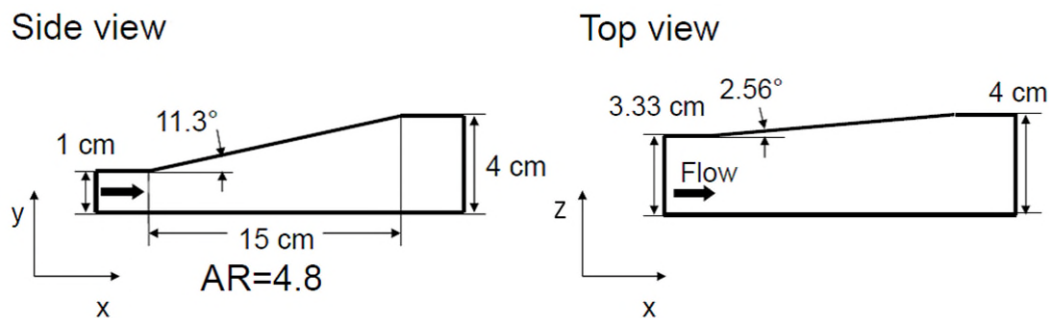


Figure 6: Geometry and dimensions of the test-case diffuser [10].

3.1 Computational domain and boundary conditions

The solution domain comprised part of the inflow duct (5H), the diffuser (15H) and a straight outlet duct (55H) (Figure 7). The origin of the coordinate system was placed at the intersection of the non-expanding walls at the inlet of the diffuser. The fully developed inflow velocity profile was generated by running a streamwise-periodic flow simulation of a duct with the same size as the diffuser inlet. Experiments show that such flows are statistically symmetric about the mid-planes [16]. Since Reynolds-averaged Navier-Stokes (RANS) turbulence models were used in this study, a quarter of the periodic duct was modelled and symmetry boundary conditions were used. The periodic duct was only a few cells long (0.2H) since RANS turbulence models do not resolve the scales of the turbulent structures.

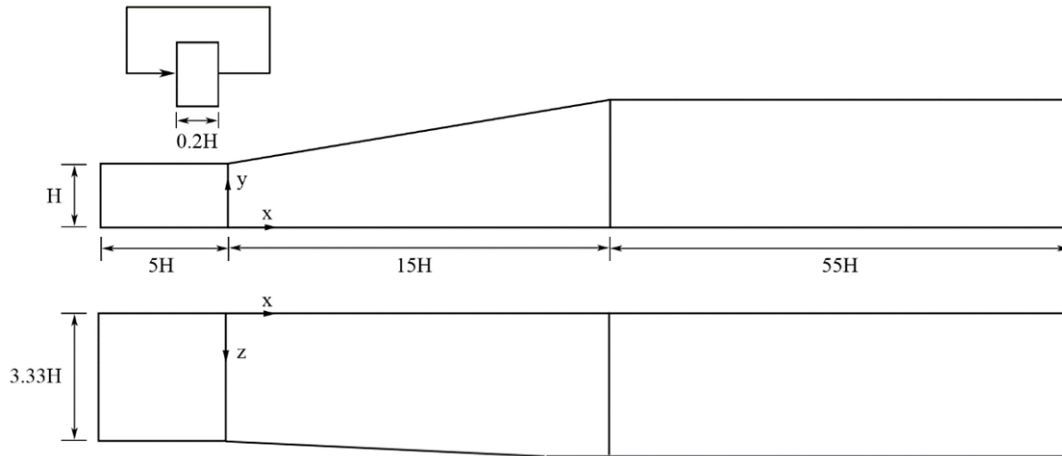


Figure 7: Schematic of the computational domain (diagram not to scale).

The fully developed turbulent velocity profile was then applied at this inlet location. The outlet of the diffuser was extended to $55H$ and an outflow boundary condition was applied. At an outflow boundary, the diffusion flux for all flow variables is assumed to be zero. This is only true for a fully developed flow; however, this condition can also be applied where the flow is not fully developed provided that the effects on the solution are small. Therefore, the length of the outlet channel was obtained by varying the outlet position until changes in the solution were negligible.

The computational domain was discretised using a hexahedral grid (Figure 8). A grid stretching ratio of 1.2 was used and the wall boundary layer was resolved with y^+ values of $\mathcal{O}(1)$. A grid convergence study was carried out using three grid sizes, each time monitoring the pressure coefficient at $x/L=1$ (Figure 9). The difference in pressure coefficient between the medium and fine grids was only 1.3% compared to 4% difference between the coarse and medium grids.

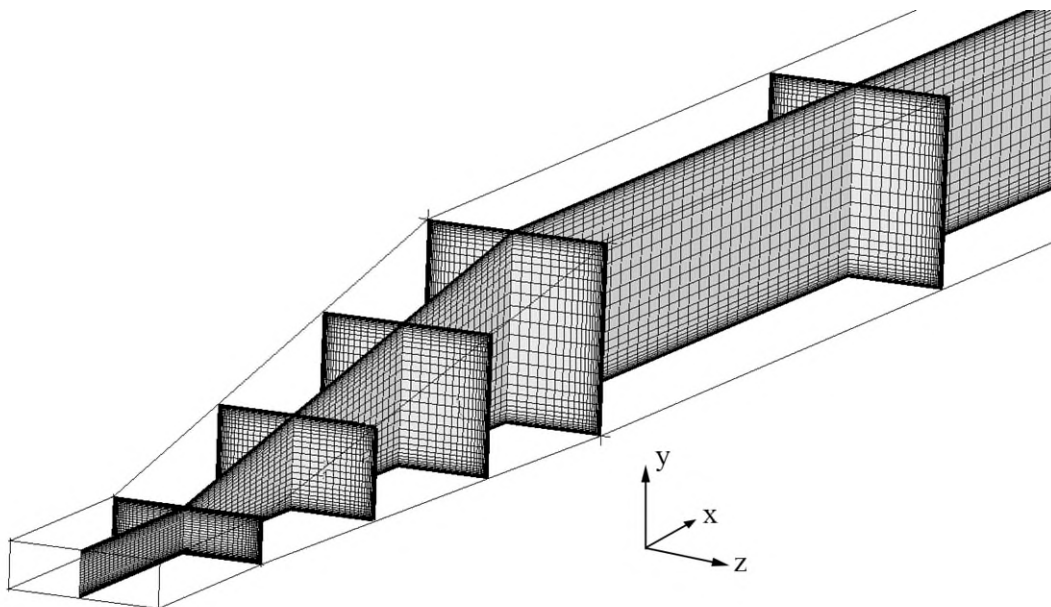


Figure 8: Grid distribution in the diffuser (medium grid).

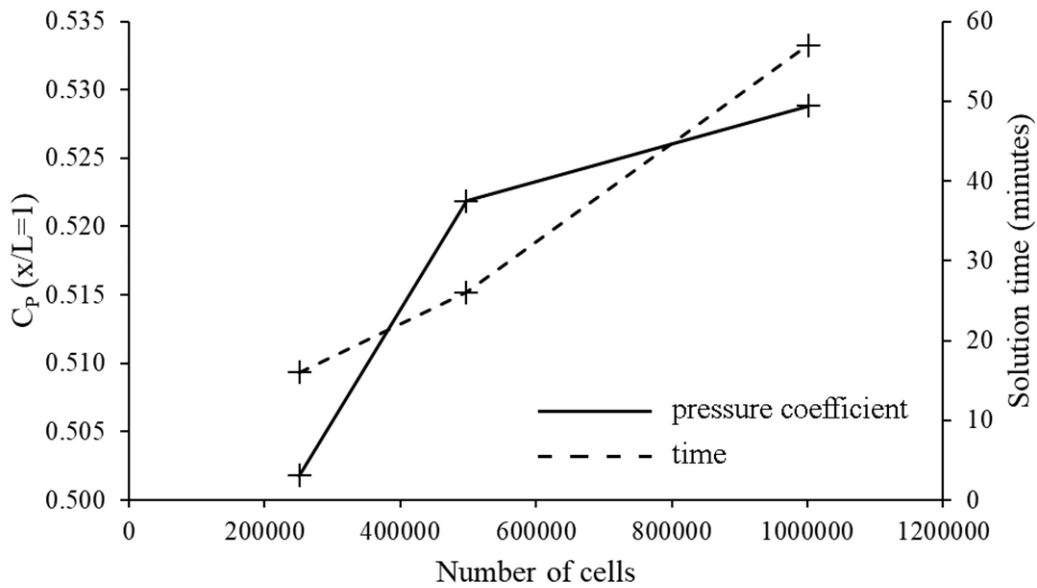


Figure 9: Grid convergence study for the periodic duct. The convergence of the pressure coefficient at $x/L = 1$ (solid line) was monitored together with the computational time (dashed line).

3.2 Results and discussion

The first step of the solution was to generate inflow velocity profiles to provide the inlet boundary conditions. Figure 10 shows half of the axial velocity profile in the vertical plane of the inflow duct for different turbulence models. The universal turbulent velocity profiles in the viscous sublayer ($y^+ \leq 5$) and log-law region ($y^+ \geq 30$) are also included. The log-law is shown with the standard constants $\kappa = 0.41$ and $B = 5.2$ [16].

The velocity profiles obtained numerically corresponded to a fully-developed equilibrium flow and follow closely the logarithmic law of the wall especially close to $y^+ = 30$. The deviation from the log-law increased towards the duct's centreline. One reason is that the statistical symmetry of flow through a rectangular duct requires that the derivative of the velocity profile be zero at the centreline. The range of y^+ values for which the log-law applies also decreases with decreasing Reynolds number. The Reynolds number for this test-case was 10000 and, as expected, the log-law best fits the numerical data in the region $y^+ > 30$ and $2y/H < 0.3$ [16].

The flow in a rectangular duct is characterised by secondary motion in the plane normal to the axial direction. These secondary currents transport high momentum fluid from the interior of the duct to the corners and low momentum fluid from the corners to the interior. This motion is possible due to Reynolds stress anisotropy where gradients in Reynolds stress generate a force which induces flow in the plane normal to the duct's axial direction [16].

Linear eddy-viscosity models, such as Spalart-Allmaras (Sp-A) and k-omega Shear Stress Transport (k- ω SST), are based on the Boussinesq hypothesis which assumes that for an axial flow, the normal Reynolds stresses are equal. Therefore, secondary flow is beyond the reach of these models and only results obtained with GL (Gibson and Launder) [17] and BSL (Baseline) Reynolds Stress Models (RSMs) are presented in Figure 11.

The qualitative agreement of the numerical results (bottom-left quarter of the duct is shown) with the experiment (full duct is shown) is presented in the plots of in-plane velocity vectors (Figure 11). With RSMs, a jet of high-momentum fluid bisected the corner forming a region of strong circulation on each side. The circulation zones rotated counter to each other as shown by the opposite signs in axial vorticity. The circulation in the trapezoidal sector was stronger than that in the triangular sector. This is consistent with a smaller diffusion in the trapezoidal sector [14].

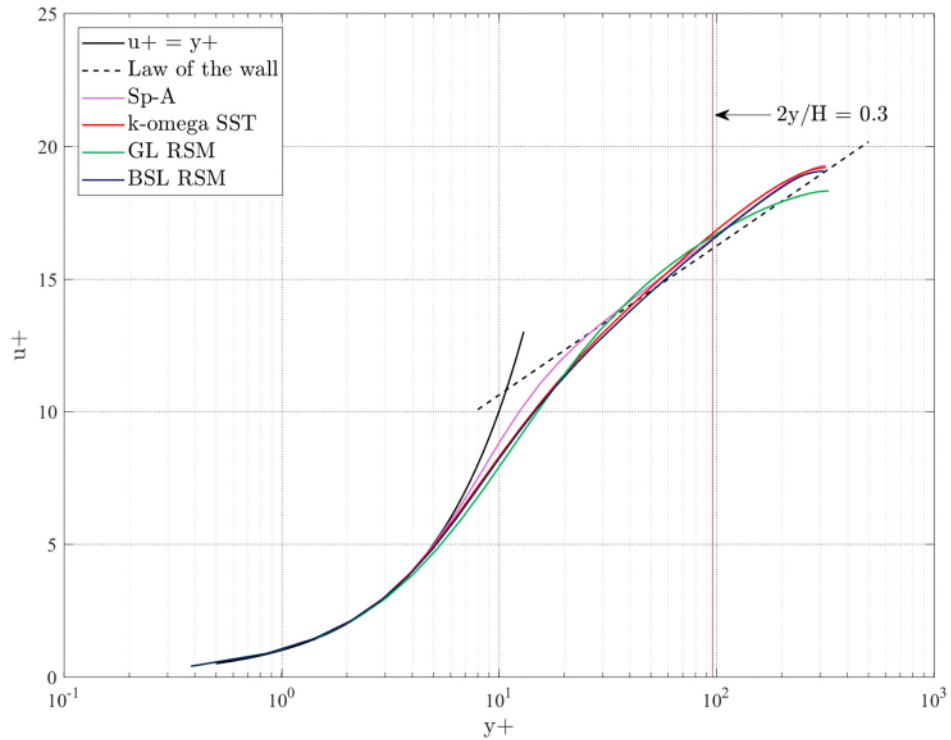


Figure 10: The figure shows half of the axial velocity profile in semi-log scale for different turbulence models together with the universal velocity profile.

A secondary weaker recirculation zone was also predicted with the GL RSM turbulence model. This extra recirculation is due to curvature reversal of the isotach near the centre of the duct in the trapezoidal area. This flow circuit was not detected by Hoagland (1960); however, as shown by the vector plot in Figure 11 (GL RSM), this recirculation is so weak that it could have been undetected by the hot-wire yaw meter [13].

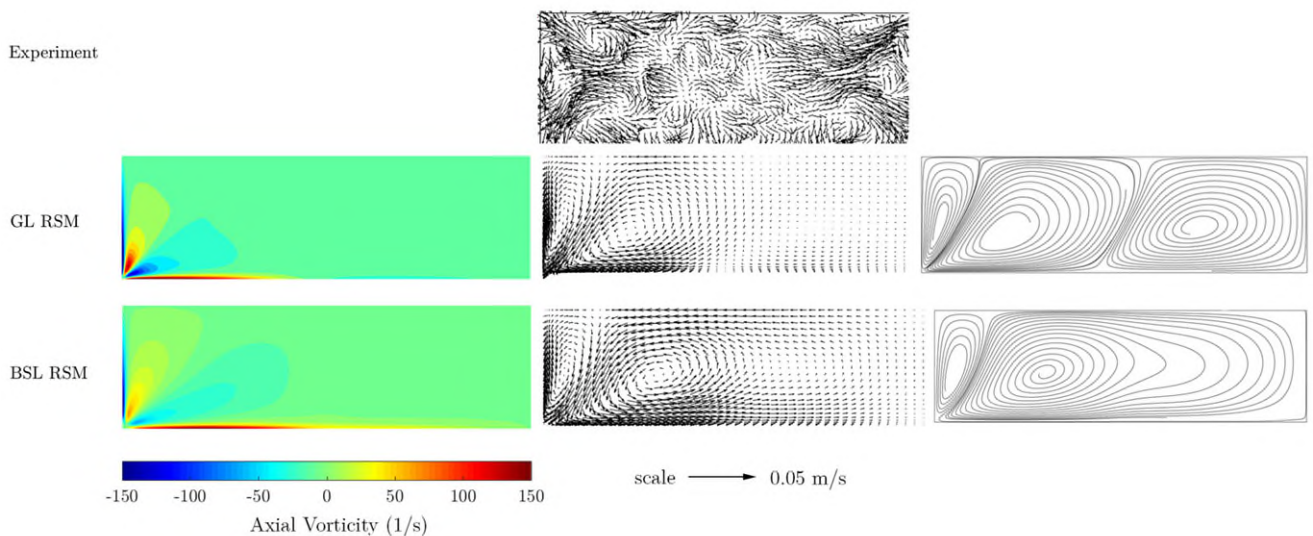


Figure 11: Turbulence-induced secondary flow in the inflow duct: plots of axial vorticity (left), in-plane velocity vectors (middle) and 2-D streamlines (right). The jet of high momentum fluid bisects the corner at approximately 45°.

In the experiment, a maximum in-plane velocity of about 0.02 m/s (2% of the bulk velocity) was measured. The uncertainty in secondary velocity measurements and direction was estimated to be less than 10% [18]. It was therefore assumed that the maximum in-plane velocity in the inflow duct of the diffuser was in the range 0.018 - 0.022 m/s. In both GL and BSL RSM models, the maximum in-plane velocity was 0.0174 m/s. This shows a good agreement between experimental and numerical results with a RSM turbulence model for the inflow duct.

The challenges of modelling flow separation in an asymmetric diffuser are due to the complexity of the strain and vorticity field. The model has to resolve complex physics including the 3-D flow separation, secondary flow of the second kind, streamline curvature and lateral straining. All linear-eddy viscosity models fail to achieve this as shown by the flow development in the diffuser (Figure 12 and Figure 13).

The two diverging walls of the diffuser imposed an adverse pressure gradient on the intersecting boundary layer in the duct, which caused it to separate. The axial velocity gradient development at two z - y planes is shown in Figure 12. The experimental velocity profile at the centre of the inflow duct was slightly asymmetric (Figure 12 top); however, this was not reproduced with any turbulence model. Since velocity was subsonic, disturbances from the diffusing flow could propagate upstream and influence the flow in the inflow duct. This could be a reason for this asymmetry and a longer inflow duct could have solved this problem.

Separation occurred immediately at the inlet of the diffuser ($x/H = 0$). Figure 13 shows contour plots of streamwise velocity at six axial locations indicating the development of the separation bubble in the diffuser with different turbulence models. For the k - ω SST, GL RSM and BSL RSM turbulence models the initial separation followed qualitatively the experimental result (Figure 13 $x/H = 2$). The result obtained with the Spalart-Allmaras model at $x/H = 2$ did not agree with the experiment since separation started at the lower-right corner. The velocity development was also significantly different where the location of maximum velocity was shifted towards the upper wall (Figure 12 top). The Spalart-Allmaras model was designed for aerospace applications with small to mild separations and this could explain its inability to predict the correct location of separation onset in this test-case [19].

Initially, the separation bubble in the experiment spread along the upper and side walls at an equal rate. However, the expansion angle of the upper wall was 11.3° while that of the side wall was 2.56° . Therefore, the adverse pressure gradient along the upper wall outweighed that on the side wall causing the separation bubble to spread gradually over the top wall.

The flow predicted in the first sections of the diffuser ($x/H \leq 4$) with a k - ω SST model compared well with the experiment in terms of mean axial velocity. However, downstream, the separation bubble evolved on the side wall instead of the upper wall. This was mainly caused by the over-sensitivity of the k - ω SST model to transverse pressure gradients. Transverse pressure gradients appear due to the expansion of the diffuser and the effect is to produce a pressure-driven secondary flow which is in general stronger than turbulence-driven secondary flow [7].

The spreading of the separation bubble over the upper surface was only captured with the BSL RSM turbulence model (Figure 13 $x/H = 15$) although the topology of the separation bubble differed from that observed experimentally. The predicted separation bubble was larger, and this had a direct effect on the pressure recovery inside the diffuser. These differences could be attributed to the intensity of the secondary flow pattern in the inflow duct, where Schneider et al. (2011) showed that even small changes in secondary velocity can have a large impact on the development of the separation bubble [20].

TURBULENCE MODEL ASSESSMENT OF THE SEPARATED FLOW IN THE STANFORD DIFFUSER

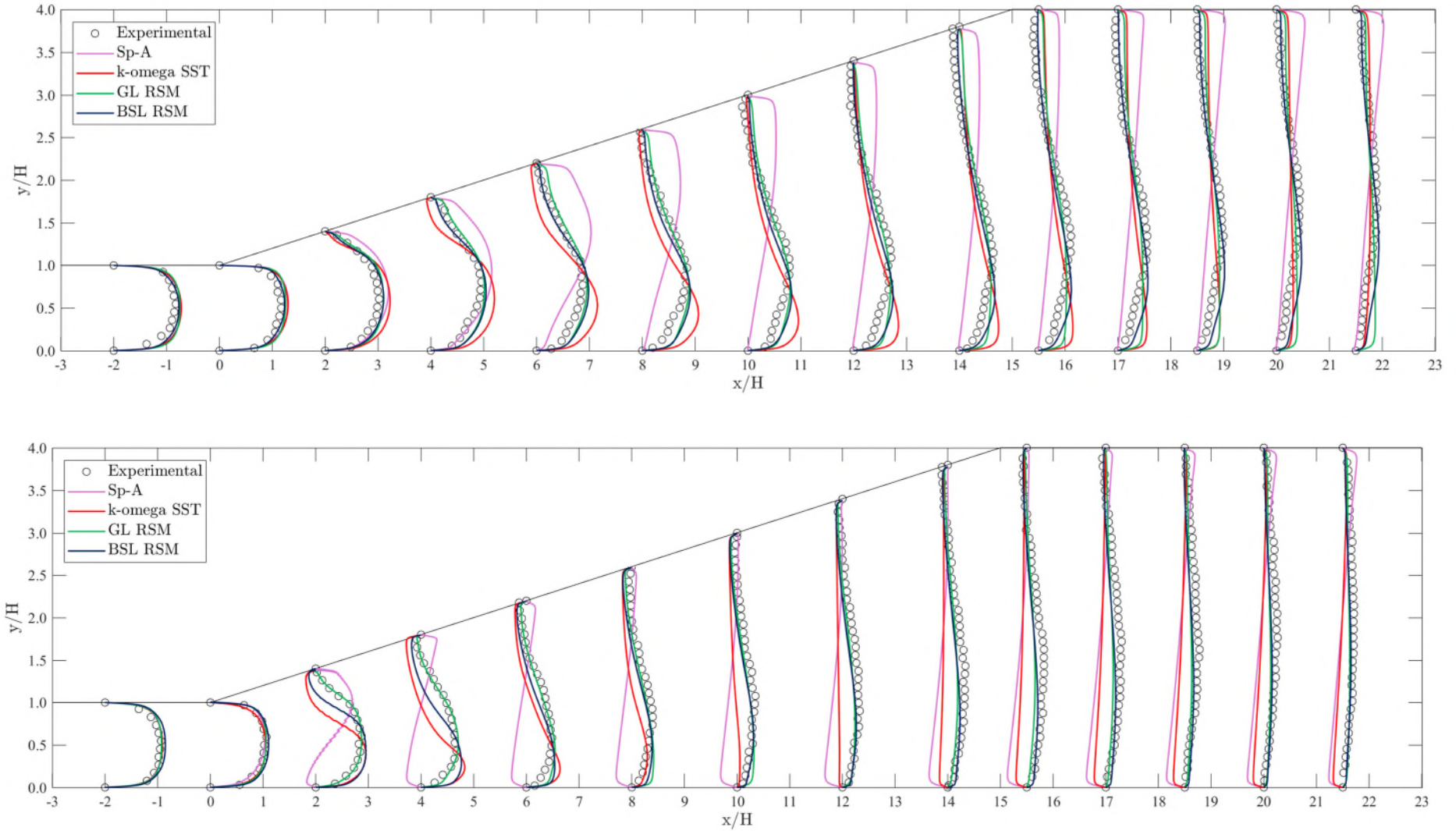


Figure 12: Development of axial velocity in the vertical plane for different turbulence models at spanwise locations of $z/B = 1/2$ (top) and $z/B = 7/8$ (bottom).

TURBULENCE MODEL ASSESSMENT OF THE SEPARATED FLOW IN THE STANFORD DIFFUSER

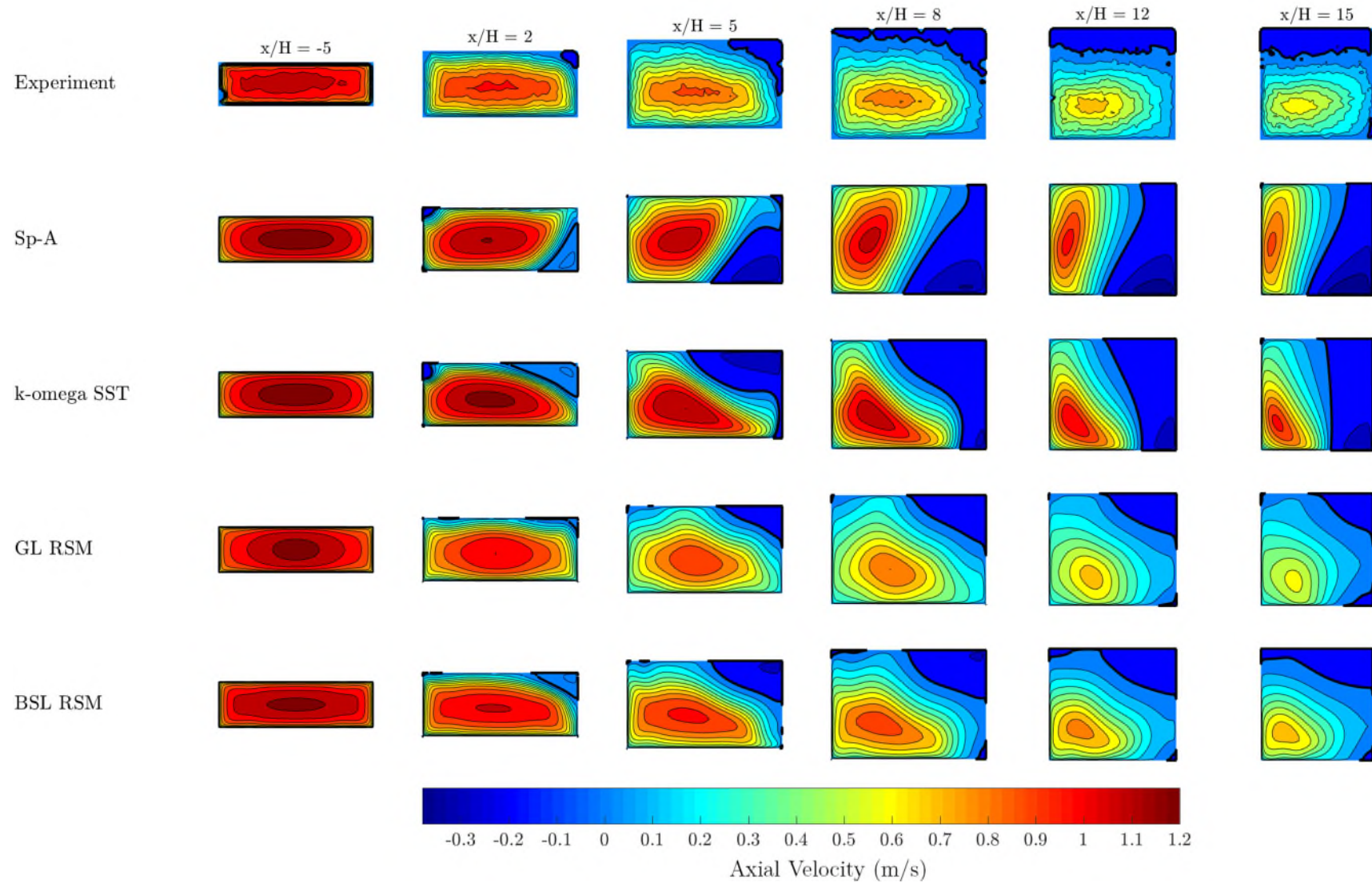


Figure 13: Streamwise velocity contours in the cross-plane z - y at six axial locations along the diffuser. The thick line marks the zero streamwise velocity contour. The dark blue areas are regions of reversed flow.

With a GL RSM turbulence model, the separation bubble occupied the upper-right corner throughout the diffuser and did not spread along the top wall (Figure 13). However, the size of the separation bubble was correct as shown by the pressure recovery inside the diffuser (Figure 14), which closely followed the experimental results. The pressure decreased in the inflow duct and started to rise rapidly near the inlet of the diffuser. Separation onset caused the flow to contract, leading to a decrease in deceleration and hence a lower pressure rise. The transition from the rapid pressure recovery to a more moderate rise occurred at $x/L=0.3$, where approximately 5% of the cross-sectional area was occupied by reversed flow.

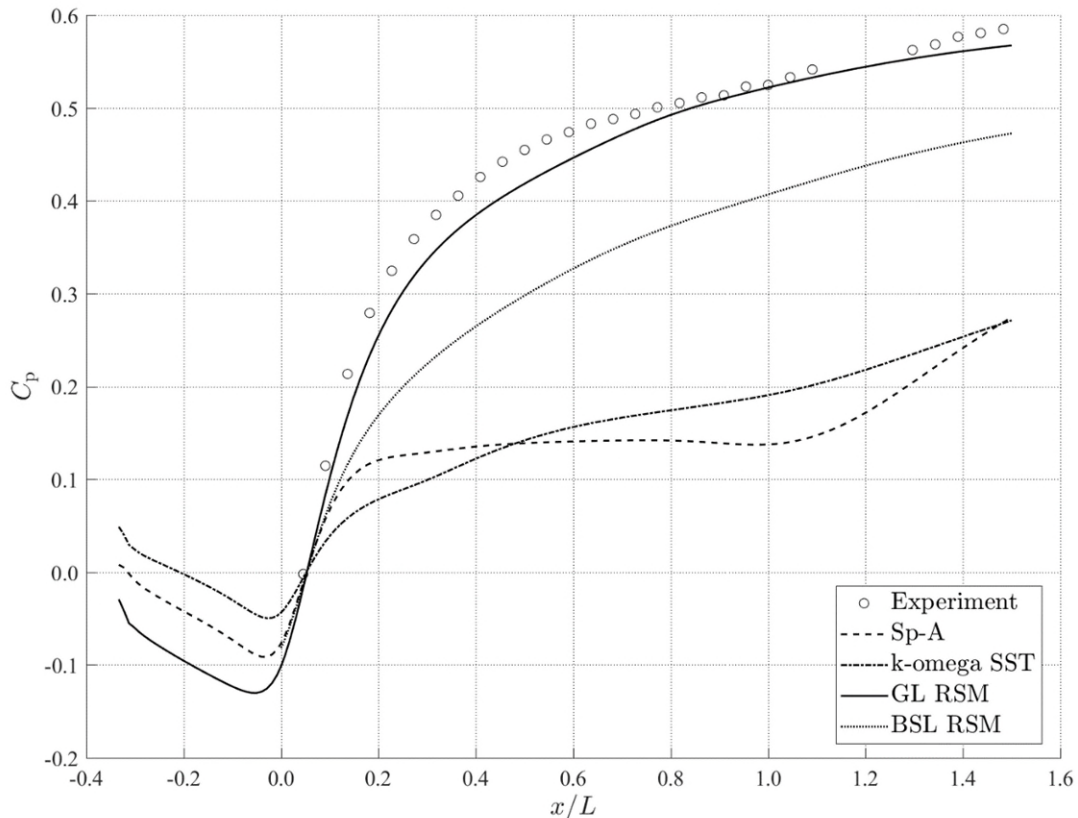


Figure 14: Recovery of pressure coefficient along the bottom wall of the diffuser. The reference pressure is the pressure at $x/H = 0.05$ and $z/B = 0.5$. The length of the diffuser is $L = 15$ cm.

Figure 15 shows plots of streamlines of secondary flow at three streamwise locations within the diffuser. The $k-\omega$ SST turbulence model cannot predict turbulence-driven secondary flow. Therefore, the secondary flow with this model was completely pressure-driven. The isotropy of the Reynolds stress tensor causes the over-sensitivity of linear eddy-viscosity models to transverse pressure gradients. On the other hand, RSMs, have a lower sensitivity to pressure-induced secondary flow since the Reynolds stress tensor can be anisotropic [7]. Therefore, the secondary flow with the GL and BSL RSM models in Figure 15 was driven both by pressure gradients and turbulence. The similarity between secondary flow patterns for GL and BSL RSM turbulence models is evident.

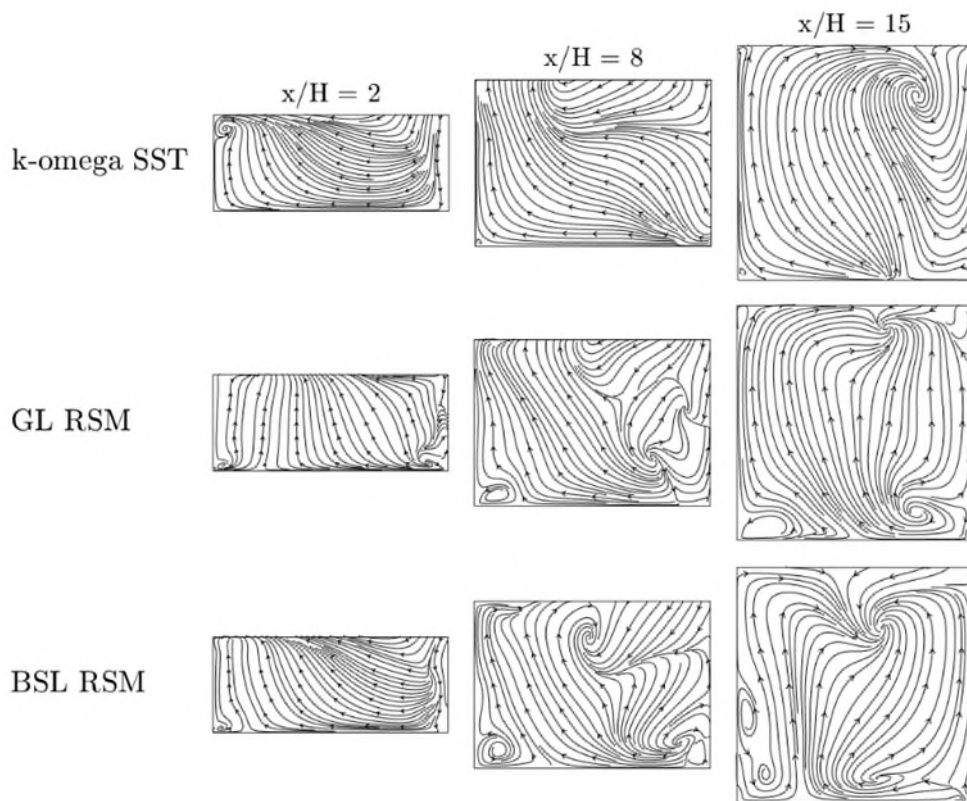


Figure 15: Streamlines of secondary flow (velocity in the z - y plane of the diffuser) at three streamwise locations predicted with the k - ω SST, GL RSM and BSL RSM turbulence models.

4. Conclusions

Three-dimensional separation is a challenge for turbulence models since many flow structures interact together to form flow separation. The 3-D separated flow in an asymmetric diffuser was studied using the test-case of Cherry et al. (2006). Results obtained with various turbulence models were compared to experimental data. The linear eddy-viscosity RANS models are over-sensitive to transverse pressure gradients. The flow close to the diffuser inlet was predicted well; however, discrepancies increased downstream. Whereas separation was located on the upper wall in the experiment, the k - ω SST model predicted separation to occur on the side wall. The linear eddy-viscosity models were also unable to predict turbulence-driven secondary flow in the inflow duct. On the other hand, the qualitative mean flowfield with RSMs was in better agreement with the experiment, although at a higher computational cost. This is due to the Reynolds Stress Models' ability to capture better the effects of streamline curvature, strain field and secondary flow in the inflow duct.

Copyright Statement

The authors confirm that they, and/or their company or organization, hold copyright on all of the original material included in this paper. The authors also confirm that they have obtained permission, from the copyright holder of any third party material included in this paper, to publish it as part of their paper. The authors confirm that they give permission, or have obtained permission from the copyright holder of this paper, for the publication and distribution of this paper as part of the ICAS proceedings or as individual off-prints from the proceedings.

References

- [1] J. Blechinger. "The influence of inlet velocity distribution on the flow through a plane curved diffuser". PhD thesis, Iowa State University, 1971.
- [2] D. G. Mabey. "Flow unsteadiness and model vibration in wind tunnels at subsonic and transonic speeds". Current Paper CP-1155, Royal Aircraft Establishment, Ministry of Aviation Supply, Bedford, 1971.
- [3] W. G. Mabey and B. L. Welsh. "The measurement of oscillatory pressures with discrete and sweep excitation. *Journal of Fluids and Structures*", Volume 1, Issue 1, pages 95-105. January 1987.
- [4] W. D. Harvey and P. C. Stainback. "Evaluation of flow quality in two large NASA wind tunnels at transonic speeds". Technical Report 1737, NASA Scientific and Technical Information Branch, 2011.
- [5] R. W. Fox and S. J. Kline. "Flow regimes in curved subsonic diffusers". *ASME Journal of Basic Engineering*, Vol. 84, pages 303–312, September 1962.
- [6] J. M. Délery. Robert Legendre and Henri Werl "Toward the Elucidation of three-dimensional separation". *Annual Review of Fluid Mechanics*, Vol. 33, pages 129–154, 2001.
- [7] E. Jeyapaul. "Turbulent flow separation in three-dimensional asymmetric diffusers". PhD thesis, Iowa State University, Department of Aerospace Engineering, 2011.
- [8] E. M. Cherry, G. Iaccarino, C. J. Elkins, and J. K. Eaton. "Separated flow in a three-dimensional diffuser: preliminary validation". Technical report, Centre for Turbulence Research, Stanford University, 2006.
- [9] E. M. Cherry, G. Iaccarino, C. J. Elkins, and J. K. Eaton. "Geometric sensitivity of three-dimensional separated flows". *International Journal of Heat and Fluid Flow*, Vol. 29, No. 3., pages 803–811, 2008.
- [10] E. M. Cherry, G. Iaccarino, C. J. Elkins, and J. K. Eaton. "Pressure measurements in a three-dimensional separated diffuser". *International Journal of Heat and Fluid Flow*, Vol. 30, No. 1, pages 1–2, 2009.
- [11] J. Nikuradse. "Investigations on the velocity distribution in turbulent flows". PhD thesis, University of Göttingen, 1926.
- [12] H. Oertel. "Prandtl – Essentials in Fluid Mechanics". Springer, 2010.
- [13] L. C. Hoagland. "Fully Developed Turbulent Flow in Straight Rectangular Ducts". PhD thesis, Massachusetts Institute of Technology, 1960.
- [14] E. Brundrett and W. D. Baines. "The production and diffusion of vorticity in duct flow". *Journal of Fluid Mechanics*, Vol. 19, No. 3, pages 375–394, 1964.
- [15] C. G. Speziale, R. M. C. So, and B. A. Younis. "On the prediction of turbulent secondary flows". NASA Technical Report TR-189722, 1992.
- [16] S. Pope. "Turbulent Flows". Cambridge University Press, 2000.
- [17] M. M. Gibson and B. E. Launder. "Ground Effects on Pressure Fluctuations in the Atmospheric Boundary Layer" *Journal of Fluid Mechanics*, Vol. 86., pages 491-511, 1978.
- [18] C. J. Elkins, M. Pelc, and J. K. Eaton. "4D magnetic resonance velocimetry for mean flow measurements in complex turbulent flows". *Experiments in Fluids*, Vol. 34, pages 494–503, 2003.
- [19] ANSYS®. FLUENT® Theory Guide, ANSYS Documentation, Release 18.32.
- [20] H. Schneider, D. von Terzi, H. J. Bauer, and W. Rodi. "Impact of secondary vortices on separation dynamics in 3D asymmetric diffusers". In *Proceedings of Direct and Large Eddy Simulation*, Eindhoven, The Netherlands, 2011.